Simulation of heat and mass transfer in turbulent channel flow using the spectral-element method: effect of spatial resolution

V Ryzhenkov[1,2], V Ivashchenko[1,2], R Vinuesa[3], R Mullyadzhanov[1,2]

[1]Institute of Thermophysics SB RAS, Novosibirsk, Russia
[2]Novosibirsk State University, Novosibirsk, Russia
[3]Linné FLOW Centre, KTH Mechanics, Stockholm, Sweden
and Swedish e-Science Research Centre (SeRC), Stockholm, Sweden

E-mail: rustammul@gmail.com

Abstract. We use the open-source code nek5000 to assess the accuracy of high-order spectral element large-eddy simulations (LES) of a turbulent channel flow depending on the spatial resolution compared to the direct numerical simulation (DNS). The Reynolds number $Re = 6800$ is considered based on the bulk velocity and half-width of the channel. The filtered governing equations are closed with the dynamic Smagorinsky model for subgrid stresses and heat flux. The results show very good agreement between LES and DNS for time-averaged velocity and temperature profiles and their fluctuations. Even the coarse LES grid which contains around 30 times less points than the DNS one provided predictions of the friction velocity within 2.0% accuracy interval.

1. Introduction

The turbulent regime of a fluid motion is often encountered in many natural phenomena and practical applications. The complexity of a turbulent flow is due to a wide spectrum of scales interacting in a non-linear fashion [1]. The problem becomes even more complicated when the flow is constrained by a rigid surface which substantially changes the properties of turbulence by introducing inhomogeneity in the wall-normal direction. The control of wall-bounded turbulent characteristics is a great scientific challenge where numerical simulations can effectively contribute.

The fluid motion is described by the Navier–Stokes equations which are nowadays possible to simulate directly resolving all the relevant scales. The obvious drawback of this approach is the high computational cost since the discretization and time step should be comparable with the size and turnover time of the smallest eddy. In a Large-eddy simulation (LES) one applies a low-pass filter to the Navier–Stokes equations. A well-known source of a possible error into the final solution is the common assumption that the spatial filtering operation commutes with spatial derivatives. The resulting equations describe the dynamics of the vortices which are larger than the filter size with a new unclosed term on the right-hand side representing the influence of the 'small' scales on the 'larger' ones. The subgrid scale model is a second source of error. The last issue in LES is the numerical scheme of discretization which brings the third kind of error. All three types of errors can interact with each other. Various approaches and

criteria have been suggested in the literature to assess the quality of LES, such as Refs. [2–7] among others. In the present work we employ a high-order spectral element method [8] to discretize the equations, thus, significantly reducing the discretization error in the final solution, and investigate the performance of the widespread dynamic Smagorinsky model for the subgrid stress tensor and heat flux vector. We perform a set of Large-eddy simulations with different levels of grid refinement using the open-source spectral element code nek5000 [9] and compare the results with DNS.

2. The governing equations and computational details

The governing equations are the following:

$$\frac{\partial \boldsymbol{u}}{\partial t} + (\boldsymbol{u}\nabla)\boldsymbol{u} = -\nabla p + \frac{1}{Re}\nabla^2\boldsymbol{u}, \qquad \nabla \cdot \boldsymbol{u} = 0, \tag{1}$$

$$\frac{\partial \theta}{\partial t} + (\boldsymbol{u}\nabla)\theta = \frac{1}{Pe}\nabla^2\theta, \tag{2}$$

where $\boldsymbol{u}$, p and θ are the dimensionless velocity vector, pressure and temperature fields, respectively. The Reynolds number $Re = U_b H/\nu$ is defined using the bulk velocity U_b, half-width of the channel H and constant kinematic viscosity of the fluid ν. Another non-dimensional criterion is the Péclet number $Pe = U_b H/\alpha$, where α is the constant thermal diffusivity. All simulations are performed for the Prandlt number $Pr = Pe/Re = \nu/\alpha = 1$. Equations (1) and (2) are used to perform direct numerical simulations (DNS).

Applying the spatial low-pass filtering [10] denoted by tilde

$$\widetilde{\boldsymbol{u}}(\boldsymbol{x}, t) = \int G(\boldsymbol{x} - \boldsymbol{r})\boldsymbol{u}(\boldsymbol{r}, t)d\boldsymbol{r}, \tag{3}$$

where G is the filter function, to equations (1) and (2) we arrive to the filtered Navier–Stokes equations:

$$\frac{\partial \widetilde{\boldsymbol{u}}}{\partial t} + (\widetilde{\boldsymbol{u}}\nabla)\widetilde{\boldsymbol{u}} = -\nabla\widetilde{p} + \frac{1}{Re}\nabla^2\widetilde{\boldsymbol{u}} - \nabla \cdot \tau, \qquad \nabla \cdot \widetilde{\boldsymbol{u}} = 0, \tag{4}$$

$$\frac{\partial \widetilde{\theta}}{\partial t} + (\widetilde{\boldsymbol{u}}\nabla)\widetilde{\theta} = \frac{1}{Pe}\nabla^2\widetilde{\theta} - \nabla \cdot \boldsymbol{q}, \tag{5}$$

where τ denotes the subgrid stress tensor and $\boldsymbol{q}$ represents the subgrid heat flux vector:

$$\tau = \widetilde{\boldsymbol{u} \cdot \boldsymbol{u}} - \widetilde{\boldsymbol{u}} \cdot \widetilde{\boldsymbol{u}}, \qquad \boldsymbol{q} = \widetilde{\boldsymbol{u}\,\theta} - \widetilde{\boldsymbol{u}}\,\widetilde{\theta}, \tag{6}$$

The subgrid stress tensor and heat flux vector are expressed using the Boussinesq hypothesis:

$$\tau_{ij} - \tau_{kk}\delta_{ij}/3 = -2\nu_t\widetilde{S}_{ij}, \qquad \nu_t = (C_s\Delta)^2|\widetilde{S}|, \qquad q_i = -Pr_t^{-1}\nu_t\,\partial_i\widetilde{\theta}, \tag{7}$$

where δ_{ij} is the Kronecker delta, ν_t, C_s and Pr_t are the turbulent viscosity, Smagorinsky constant and turbulent Prandtl number which are computed dynamically as described below, Δ is the filter width, and $|S| = \sqrt{2S_{ij}S_{ij}}$ is the magnitude of the strain-rate tensor

$$S_{ij} = \frac{1}{2}(\partial_j u_i + \partial_i u_j), \tag{8}$$

where a compact notation for the derivative is adopted, $\partial_j u_i = \partial u_i/\partial x_j$. The Smagorinsky constant and turbulent Prandtl number are defined as follows [11, 12]:

$$C_s^2 = -\Big\langle \Big(\widehat{\widetilde{u}_i\widetilde{u}_j} - \widehat{\widetilde{u}}_i\widehat{\widetilde{u}}_j\Big)\widetilde{S}_{ij}\Big\rangle \Big/ \Big\langle 2\Big(\widehat{\Delta}^2|\widehat{\widetilde{S}}|\widehat{\widetilde{S}}_{ij} - \Delta^2\widehat{|\widetilde{S}|\widetilde{S}_{ij}}\Big)\widetilde{S}_{ij}\Big\rangle, \tag{9}$$

$$Pr_t = C_s^2\left[\Big\langle \Big(\widehat{\widetilde{u}_i\widetilde{\theta}} - \widehat{\widetilde{u}}_i\widehat{\widetilde{\theta}}\Big)\partial_i\widetilde{\theta}\Big\rangle \Big/ \Big\langle \Big(\widehat{\Delta}^2|\widehat{\widetilde{S}}|\partial_i\widehat{\widetilde{\theta}} - \Delta^2\widehat{|\widetilde{S}|\partial_i\widetilde{\theta}}\Big)\partial_i\widetilde{\theta}\Big\rangle\right]^{-1}, \tag{10}$$

where the angular brackets ($\langle\ .\ \rangle$) denote the averaging along the homogeneous directions (x and z in our case, see Fig. 1 below). Thus, C_s and Pr_t are the functions of time and one spatial (wall-normal) direction only. The value of the Smagorinsky constant is clipped to zero in case the negative values occur. The test filter $\widehat{\Delta} = 2\Delta$ in the position (x_i, y_i, z_i) is defined as $\sqrt[3]{\Delta x_i \Delta y_j \Delta z_k}$, where $\Delta x_i = x_{i+1} - x_{i-1}$, $\Delta y_j = y_{j+1} - y_{j-1}$, $\Delta z_k = z_{k+1} - z_{k-1}$ with i, j, k being the structured indices of the point inside each spectral element. The above described governing equations are implemented in the nek5000 code [9] with a spatial discretisation based on the spectral-element method using Lagrange polynomials. The Navier–Stokes equations are cast in a weak form and discretised in space by means of Galerkin approximation using Nth-order Lagrange polynomial interpolants on the Gauss-Lobatto-Legendre points for the velocity field and $(N-2)$th-order for the pressure ($\mathbb{P}_N - \mathbb{P}_{N-2}$ formulation). In the present work the polynomial order N is set to 7. The semi-implicit time-stepping scheme is of the third-order accuracy.

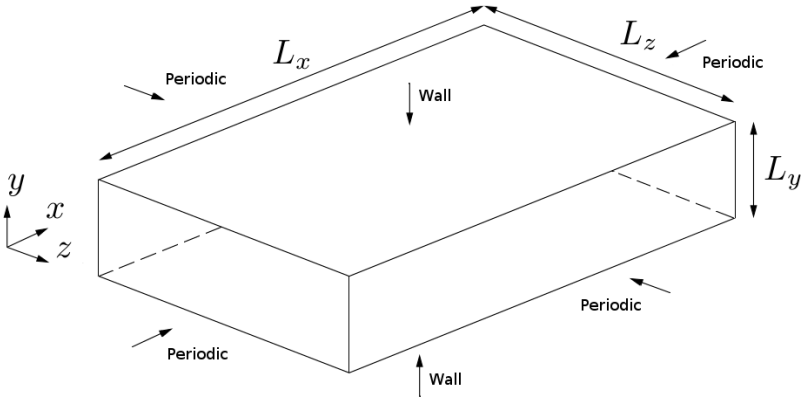

Figure 1. Geometry of the channel and boundary conditions

We study a turbulent flow between two infinite parallel walls at a Reynolds number of $Re = 6800$. A rectangular computational domain of the size $L_x \times L_y \times L_z = 2\pi H \times 2H \times \pi H$ is used where x is the streamwise coordinate (along the flow), y is the wall-normal axis and z is the spanwise coordinate, Fig. 1. The planes $y = \pm H$ correspond to the position of parallel walls. The infinite flow domain is modeled by periodic boundary conditions in x and z directions. No-slip condition ($\boldsymbol{u} = 0$) and constant temperature for hot upper ($\theta = \theta_h$) and cold lower ($\theta = \theta_c$) wall are imposed. A dynamically adjusted body force is added in equations (1) and (3) to keep a constant mass flux through the plane $y - z$. Note that all the quantities below are non-dimensionalized using U_b, $\Delta\theta = \theta_h - \theta_c$ and H unless otherwise specified.

The initial conditions of the simulation are set using the analytic profiles $u_x = 5(1 - y^4)/4$, $u_y = u_z = 0$ and $\theta = (1 + y)/2$. The random noise with a 5% amplitude of the bulk velocity is added to all velocity components to accelerate the transition to turbulence. The statistical analysis is performed for the flow only after a sufficient period of computational time to minimize the influence of initial transients on time-averaged characteristics. Figure 2 shows the instantaneous temperature field of the flow going from left to right from the DNS visualizing the near-wall vortical structures. Table 2 shows the characteristics of the mesh used for DNS and LES, where N_{se} is the number of spectral elements along each direction (x, y, z), N_{points} is the number of nodes along each direction and N_{tot} is the total number of nodes. We used structured hexahedral grids for the present calculations.

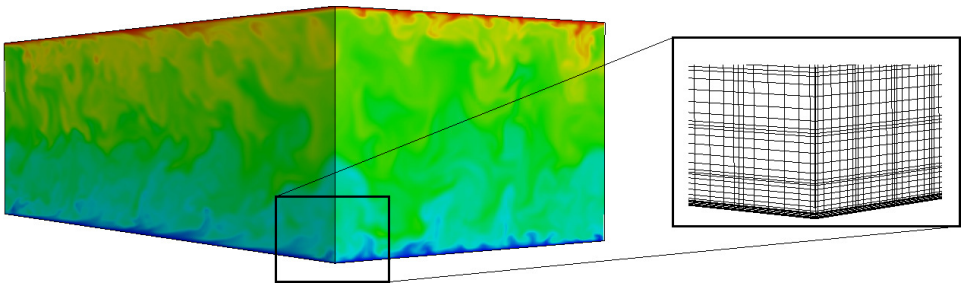

Figure 2. Instanteneous temperature field from DNS. The flow goes from left to right. The top wall is hot (red), the bottom one is cold (blue). The inset on the right shows a small fragment of the computational hexahedral mesh

Table 1. Mesh characteristics

	DNS	LES1	LES2	LES3
N_{se}	$40 \times 30 \times 30$	$26 \times 20 \times 20$	$20 \times 16 \times 16$	$14 \times 10 \times 10$
N_{points}	$320 \times 240 \times 240$	$208 \times 160 \times 160$	$160 \times 128 \times 128$	$112 \times 80 \times 80$
N_{total}	18.4×10^6	5.3×10^6	2.6×10^6	0.72×10^6

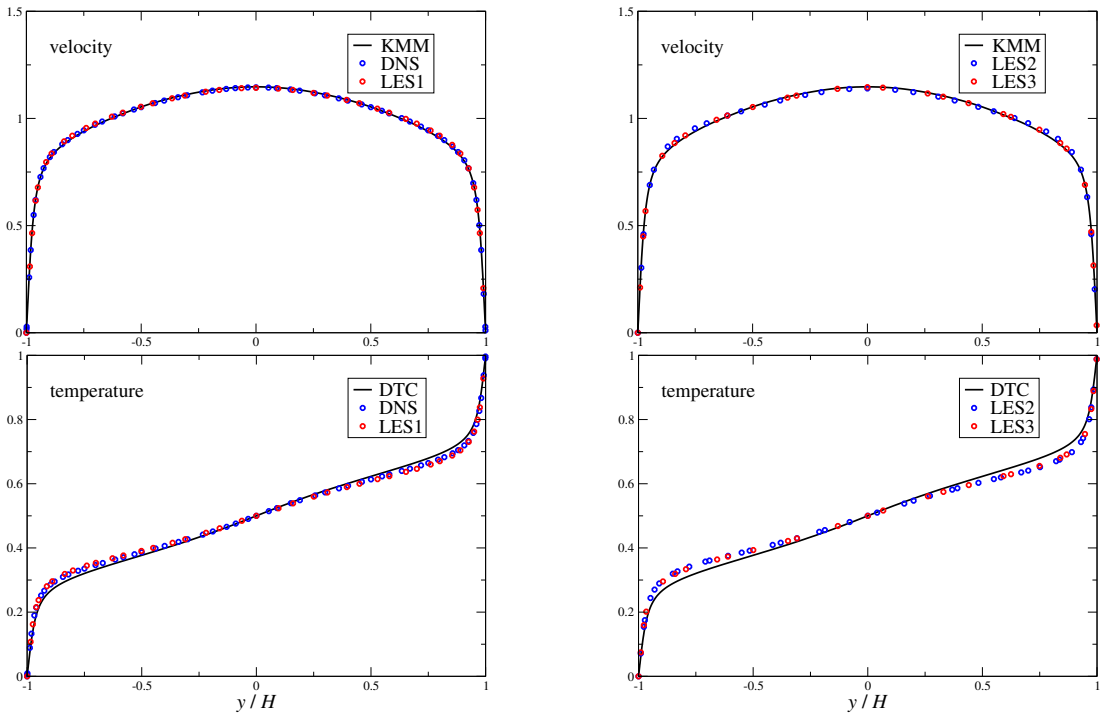

Figure 3. Comparison of the time-averaged velocity and temperature profiles with the data from KMM [13] and DTC [14]

3. Results

We compare time-averaged profiles of velocity, temperature and its fluctuations from the present DNS, LES and DNS data from the literature [13, 14]. The present data is also averaged along the homogeneous x and z directions. Figure 3 shows the comparison of $\overline{u}_x$ and $\overline{\theta}$ where the

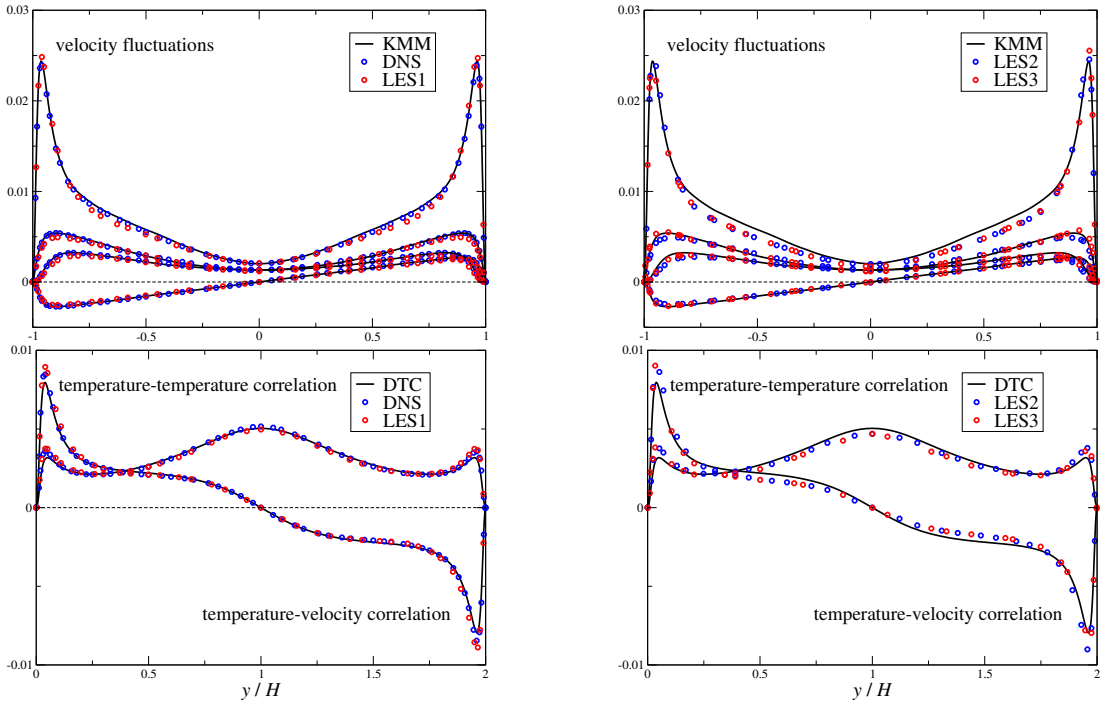

Figure 4. Comparison of the time-averaged velocity and temperature fluctuations with the data from KMM [13] and DTC [14]

overline denotes the time-averaging. The velocity profile is in excellent agreement with the data of [13] who used a fully spectral code based on Chebyshev polynomials in y and Fourier in x and z direction. The temperature profile also shows good agreement, however, slightly deviating from the data [14]. Note that in the present calculations $Pr = 1.0$ while $Pr = 0.71$ in [14] who used second order accurate discretization.

Figure 4 shows the comparison of different components of $\overline{u_i' u_j'}$ and $\overline{u_i' \theta'}$. DNS shows excellent agreement, while the LES data may slightly deviate from the results of [14]. The important fact is a good prediction of the fluctuations peak near the wall even for the very coarse mesh (LES3). This peak is the result of the dynamics of streaky structures in the near-wall region. Figure 5 shows the instantaneous field of u_x near the wall ($y/H = 0.95$) in the $x-z$ plane, where this peak of fluctuations appear. Visualizations for all meshes look very similar despite the differences in the spatial resolution. Table 3 shows the comparison of the non-dimensional friction velocity u_τ ($u_\tau^2 = Re^{-1} \partial_y \overline{u}_x|_{wall}$) and friction temperature $\theta_\tau = (Pe\ u_\tau)^{-1} \partial_y \overline{\theta}|_{wall}$. All simulations show excellent agreement with data from the literature within 2.0% accuaracy interval. Note that relatively high u_τ deviation calculated for LES1 mesh is probably caused by the effect of transients and insufficient averaging time. This issue is currently investigated. Note also the robust prediction of the correct θ_τ value for all grids even when u_τ deviates (LES1). The larger value of θ_τ in [14] is due to the lower Pe (0.71 against 1.0).

4. Conclusion

We performed a series of Large-eddy simulations of a turbulent channel flow at $Re = 6800$ to assess the accuracy of the numerical method coupled with dynamic Smagorinsky model for subgrid stress tensor and heat flux vector. An excellent agreement for the time-averaged velocity,

Table 2. Comparison of u_τ and θ_τ (percentage is given as a relative error in comparison with the present DNS data)

	[13, 14]	DNS	LES1	LES2	LES3
u_τ	0.05699	0.05701	0.05588 (-1.98%)	0.05663 (-0.67%)	0.05634 (-1.18%)
θ_τ	0.02306	0.01945	0.01933 (-0.62%)	0.01962 (+0.87%)	0.01981 (+1.85%)

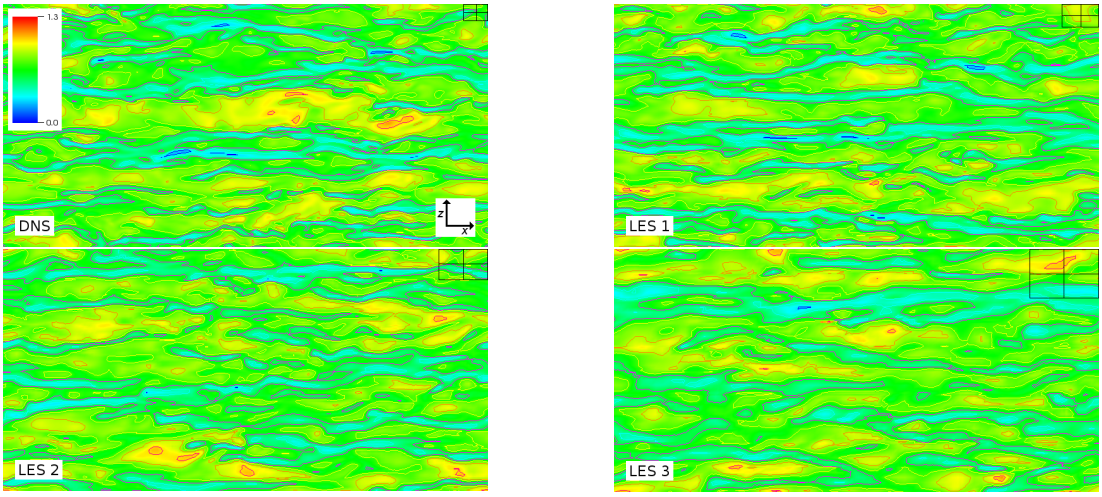

Figure 5. Instantaneous axial velocity field in $x-z$ plane near the wall at $y/H = 0.96$ ($y^+ = yu_\tau/\nu \approx 16$) for DNS and LES is shown. In the right top corner four spectral elements are shown schematically

temperature and their fluctuations is obtained. We also compared the value of friction velocity and temperature indicating the near-wall solution accuracy. Even the coarse LES grid which contains around 30 times less points than the DNS one provided predictions of the friction velocity within 2.0% accuracy interval which is encouraging for engineering applications. The next step is to assess the accuracy of LES in variable-density flows. Spectral-element method is well suited for procedures such as spatial filtering and deconvolution employed in reacting flow models [15].

Acknowledgments

This work is funded by the Russian Science Foundation grant No. 14-19-01685. The computational resources are provided by Siberian Supercomputer Center SB RAS (Novosibirsk).

References

[1] Landau LD, Lifshitz EM 1982 *Fluid Mechanics* (New York: Pergamon)
[2] Geurts BJ, Fröhlich J 2002 A framework for predicting accuracy limitations in large-eddy simulation *Phys. Fluids* **14**(6) 1070-6631
[3] Meyers J, Geurts BJ, Baelmans M 2003 Database analysis of errors in large-eddy simulation *Phys. Fluids* **15**(9) 1070-6631
[4] Klein M 2005 An attempt to assess the quality of Large Eddy Simulations in the context of implicit filtering *Flow Turb. Comb.* **75** 131–147
[5] Celik IB, Cehreli ZN, Yavuz I 2005 Index of resolution quality for Large Eddy Simulations *J. Fluids Engrg.* **127**(5) 949–958
[6] Meyers J, Geurts BJ, Sagaut P 2007 A computational error-assessment of central finite-volume discretizations in large-eddy simulation using a Smagorinsky model *J. Comp. Phys.* **227** 156–173

[7] van der Bos F, Geurts BJ 2010 Computational error-analysis of a discontinuous Galerkin discretization applied to large-eddy simulation of homogeneous turbulence *Comput. Methods Appl. Mech. Engrg.* **199** 903–915
[8] Deville MO, Fischer PF, Mund EH 2002 *High-order methods for incompressible fluid flow* (Cambridge University Press)
[9] Fischer P, Lottes J, Kerkemeier S Nek5000 web page (http://nek5000.mcs.anl.gov)
[10] Sagaut P 2006 *Large Eddy Simulation for Incompressible Flows: An Introduction* (Springer Science & Business Media)
[11] Germano M, Piomelli U, Moin P, Cabot WH 1991 A dynamic subgridscale eddy viscosity model *Phys. Fluids A* **3**(7) 1760-5
[12] Moin P, Squires K, Cabot W, Lee S 1991 A dynamic subgridscale model for compressible turbulence and scalar transport *Phys. Fluids A* **3**(11) 2746-57
[13] Moser RD, Kim J, Mansour NN 1999 Direct numerical simulation of turbulent channel flow up to $Re_\tau = 590$ *Phys. Fluids* **11**(4) 943–945
[14] Dharmarathne S, Tutkun M, Araya G, Castillo L 2016 Structures of scalar transport in a turbulent channel *Eur. J. Mech. B/Fluids* **55** 259–271
[15] Domingo P, Vervisch L 2015 Large Eddy Simulation of premixed turbulent combustion using approximate deconvolution and explicit flame filtering *Proc. Comb. Inst.* **35** (2) 1349–1357